Preparation, Characterization, and Properties of Exfoliated/Delaminated Organically Modified Clay/Dicyclopentadiene Resin Nanocomposites

Mitra Yoonessi,[†] Hossein Toghiani,[†] William L. Kingery,[§] and Charles U. Pittman, Jr.*[,‡]

Dave C. Swalm School of Chemical Engineering, Departments of Chemistry and Plant and Soil Sciences, Mississippi State University, Mississippi State, Mississippi 39762

Received December 18, 2003; Revised Manuscript Received January 26, 2004

ABSTRACT: Highly delaminated poly(dicyclopentadiene)/clay nanocomposites were synthesized by in situ polymerization of dicyclopentadiene/organically modified montmorillonite clay dispersions. Dicyclopentadiene/clay suspensions were sonicated for various times to enhance the degree of delamination prior to curing. The *d* spacings of the clay in nanocomposites were monitored using X-ray diffraction (XRD), and the extent of delamination was examined by transmission electron microscopy (TEM) and preliminary neutron scattering studies. A new approach, use of confocal laser microscopy, was employed to follow the dispersion of clay layers, tagged by a fluorescent dye, within the liquid monomer. It is evident that XRD cannot be used alone as a criterion for exfoliation. TEM showed that increasing the clay concentration at constant sonication gave an increase in average tactoid size. The largest improvement in composite mechanical properties occurred at clay loading levels (0.5−1 wt %). Significant increases in T_g, elastic bending moduli, flexural moduli, and flexural strengths were found at 0.5−1 wt % clay loadings, where the highest degree of delamination/exfoliation also occurred.

Introduction

Hybrid organic−inorganic materials have shown superior physical mechanical properties compared to conventional materials.[1−8] To optimize the performance of these materials, it is usually desirable to disperse the inorganic component within the organic component at the nanoscale level.[9−11] Polymer-layered silicate nanocomposites, containing small amounts of the inorganic phase, have exhibited superior properties to those of the pure polymers. For example, modulus, strength, thermal expansion coefficient, toughness, gas permeability barrier, and flammability resistance all may be improved.[12−17] Montmorillonite (MMT) is a crystalline, 2:1 layered clay mineral. A single layer of this clay has a central alumina octahedral sheet, which is sandwiched between two silica tetrahedral sheets.[18] By overcoming the forces between layers, small molecules may enter into clay galleries and be polymerized.[19,20]

In general, the polymer/clay composites can be divided into three categories: (1) conventional composites in which clay tactoids and particles exist in their original aggregated states, (2) intercalated nanocomposites where individual platelets are interlayered by a few polymer molecules, and (3) exfoliated nanocomposites, where individual 1 nm thick clay layers are separated in the continuous polymer/matrix.[12,14,16] Another category can be defined which makes a distinction between fully exfoliated nanocomposites and intercalated nanodispersions. This category can be called the highly delaminated nanocomposites. In fully exfoliated nanocomposites, clay layers are well dispersed as 1 nm thick noninteracting clay layers. However, in highly delaminated nanocomposites, stacks of about 2−20 layers of clay (small tactoids) are well dispersed in the polymer matrix. In this type, the XRD peak of the ordered structure disappears despite the fact that stacked layers still exist.[21,22] We are not aware of any reports demonstrating completely exfoliated clay nanocomposites.

Three main approaches have been used to form clay nanocomposites: melt blending, solution blending, and in situ polymerization.[11,12,14,16] In this paper, we report the partial exfoliation of organically modified montmorillonite clay to a highly delaminated state in the low-viscosity, nonpolar monomer, dicyclopentadiene (DCPD), followed by an in situ ring-opening polymerization/curing which captures this highly delaminated clay in a cross-linked polymer network. The delamination process was aided by sonication in some cases.

Experimental Section

Materials. The organically treated montmorillonite clays, Nanomer I-28 modified with trimethyloctadecylammonium ion and Nanomer I-44pa modified with dimethyldidecylammonium ion, were used as received in this work. The clays were purchased from Nanocor, Inc. Greater than 95% of all ions had been exchanged for the quaternary ammonium ions. Both I-28 and I-44pa exhibited *d* spacings of 2.56 nm. DCPD (purity of 99.2%) was obtained from Cymetech, LLC, under the name brand of Ultrene99. Cyclopentadiene (CPD) (4 wt %) was added to the pure DCPD. This monomer combination was used in all of the composites. Pure DCPD melts at 39 °C. The presence of small amounts of cyclopentadiene lowers the melting point of DCPD below room temperature, which allowed mixing and sonication of the clay with the monomer to be carried out at room temperature.

Dichloro(3-methyl-2-butenylidene)bis(tricyclopentyl)phosphine ruthenium (a Grubbs-type catalyst),[26,27] obtained from Cymtech LLC, was employed as the ring-opening metathesis polymerization (ROMP) catalyst.[23−27] Safranine O, a fluorescent dye, was used to tag clay layers in the I-28 clay/DCPD dispersion. Safranine O (4 g in 200 mL of denatured alcohol and water) was obtained from Becton Dickinson and used as received.

Preparation of Nanocomposites. Highly delaminated DCPD/nanoclay composites were prepared by dispersing the

[†] Dave C. Swalm School of Chemical Engineering.
[‡] Departments of Chemistry.
[§] Plant and Soil Sciences.
* Corresponding author: Tel 662 325 7616; Fax 662 325 7611; e-mail cpittman@ra.msstate.edu.

10.1021/ma0359483 CCC: $27.50
Published on Web 03/09/2004

clay (0.5−5 wt %) into the liquid DCPD and then polymerizing/curing the DCPD to form the solid composite. Clay I-28 was dispersed in liquid DCPD by stirring for 1 h followed by sonication for 3 h under nitrogen at 20 kHz and a wave amplitude of 30 using a 500 W sonication model GE501 ultrasonic processor (Ace Glass Inc.). Each sonication batch contained 10−15 g of the clay I-28/DCPD dispersion. Samples (8−10 g of dispersion) were cured by adding the Ru-based catalyst (0.018 75 g of catalyst/10 g of monomer; DCPD/catalyst mole ratio of 2860) to the nanodispersion and subsequent heating. Mole fractions of catalyst less than 0.0002 are sufficient.[23−27] A few droplets of methylene chloride were added to the catalyst to wet the surface. Then the DCPD/clay nanodispersion was added to the wetted catalyst, followed by mixing for 3−5 min. An exothermic polymerization reaction started at room temperature, and then the viscous polymerizing dispersion was poured into preheated (76 °C) steel mold where gelation occurred as the cure continued within about 2−3 min. The mold was placed into a hot press at 1 atm for 15 min at 76 °C, 25 min at 138 °C, 40 min at 160 °C, and finally 1 h and 15 min at 260 °C. The pressure was increased to 5 atm when the temperature increased to 260 °C during molding. All samples used in mechanical property testing were also postcured for 2 h at 280 °C under high-purity helium.

I-44pa clay/polyDCPD nanocomposites were prepared by stirring I-44pa into DCPD for 1 h without sonication. These dispersions were then cured by the same protocol used for the I-28 composites.

X-ray Diffraction Measurements. XRD analysis was used to follow the clay's d spacing in the cured nanocomposites vs the extent of mixing and sonication used during dispersion. XRD data on clay powder and nanocomposites samples were collected on a Philips diffractometer, model X'Pert, using Cu Kα radiation ($\lambda = 0.154\ 056$ nm). Scans were taken over the 2θ range of 1−10°, with a step size of 0.03° at 1 s per step.

Small-Angle X-ray Scattering. SAXS experiments were performed on the Oak Ridge National Laboratory's (ORNL) 10 m SAXS instrument,[28,29] with a sample−detector distance of 1.119 m using Cu Kα radiation ($\lambda = 1.54$ Å) and a 20 × 20 cm^2 two-dimensional position-sensitive area detector with each virtual cell (element) of about 3 mm apart. Corrections were made for instrumental background, dark current due to cosmic radiation and electronic noises in the detector circuitry, and the detector nonuniformity and efficiency (using an Fe^{55} radioactive isotope standard, which emits X-rays isotropically by electron capture) on a cell-by-cell basis. The data were radially (azimuthally) averaged in the Q range, $0.01 < Q < 0.4$ Å^{-1}, $Q = ((4\pi/\lambda))\sin((\theta/2))$, where λ is the X-ray wavelength and θ is the scattering angle. Then these data were converted to an absolute differential scattering cross section by means of precalibrated secondary standards.[30] The absolute scattering intensity is in cm^{-1} units.

A Molecular Metrology small-angle X-ray scattering system was used to study small-angle X-ray scattering at a sample-to-detector distance of 5 m. The X-ray source was a copper Kα, microfocused X-ray beam with a wavelength of 1.542 Å operating at 45 kV and 0.66 mA. A multiwire detector consisting of a 2-dimensional array of wires was used. The data were radially averaged and converted to an absolute differential scanning scale. The same composite samples were used in measurements with the two SAXS instruments.

Mechanical Properties. Three-Point Bending. A Zwick material testing machine (model 1435) was used for three-point bending tests to obtain flexural moduli and flexural strengths at ambient temperature. Sample thicknesses ranged from 2 to 3 mm, widths 10 to 11 mm, and lengths from 38 to 40 mm. A span of 20 mm was used in a 50 kN load cell.

DMTA. Dynamic mechanical thermal analyses was performed using a Rheometrics Scientific model MK III instrument between 50 and 320 °C at both 1 and 10 Hz using sample thicknesses from 1.5 to 2.5 mm and widths of 4−5 mm.

Transmission Electron Microscopy. A JEM-100CX II transmission electron microscope (60 kV) was used to examine clay morphology and orientation. Nanocomposite samples were ultramicrotomed to thicknesses of 70−85 nm at room temperature using a Reichert-Jung Ultracut E ultramicrotome equipped with a diamond knife. The samples were placed on a Formvar-coated 200 mesh copper grid. The clay vs polymer matrix contrast was sufficient to permit electron micrograph imaging without staining.

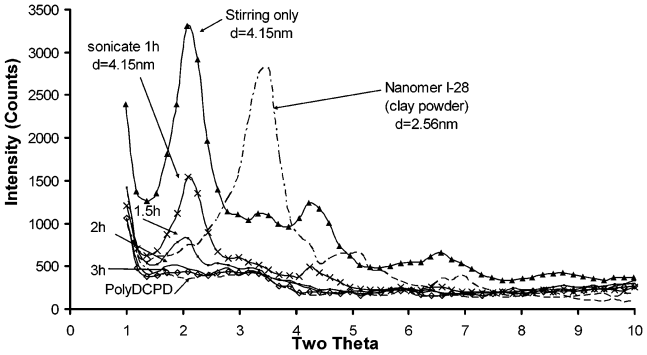

Figure 1. XRD plots of I-28 clay, polyDCPD, and 0.5 wt % I-28/polyDCPD composites delaminated by stirring or sonication.

Confocal Laser Microscopy. A Leica TCSNT confocal laser scanning microscope with laser wavelengths of 476, 488, and 568 nm was used. Clay was tagged with Safranine O, a fluorescent probe with an excitation $\lambda = 495$ nm and emission at $\lambda = 586$ nm.[31] A solution of Safranine O (4 g in 200 mL of denatured alcohol and water) was used. Then I-28 clay (0.5 g) was dispersed in 15 mL of this solution, stirred overnight, filtered, and dried. Then a 1 wt % Safranine O-tagged I-28/DCPD dispersion was made by stirring. An aliquot was sonicated for 3 h. The liquid dispersions were then analyzed.

Results and Discussion

Polymerization of DCPD. DCPD polymerizes in the presence of the Ru catalyst via a highly exothermic living ROMP mechanism.[23−27] Linear polymerization was initiated at temperatures of 40−60 °C as the strained norbornene double bond undergoes ring-opening metathesis (ROMP). This is followed by cross-linking, via metathesis of cyclopentadiene double bond, as the temperature exceeds 80 °C. The exothermic reaction and programmed heating caused the temperature to rise, and cross-linking occurred far more rapidly at 150 °C.

Delamination in PolyDCPD/Clay Nanocomposites. DCPD is a nonpolar organic monomer, requiring a montmorillonite clay that has been modified by a nonpolar organic layer in order to be exfoliated. Preliminary attempts to disperse I-28 into DCPD by stirring this clay in liquid DCPD resulted in monomer migration into the clay galleries. Gallery expansion was indicated by an increase in d spacing from 2.56 to 4.15 nm (XRD, Figure 1). Untreated sodium montmorillonite clay does not undergo gallery expansion, illustrating the ability of octadecyl hydrophilic chains to permit DCPD intercalation.

Sonication in DCPD further delaminated the I-28 clay. A series of DCPD/clay samples were cured after sonicating the clay/liquid DCPD suspensions for various times. The d spacing increased with increasing sonication time as seen from the shift of the XRD peak to smaller 2θ angles.

The intensity of the XRD basal diffraction peak also decreased, indicating delamination was proceeding. After 3 h of sonication, nanocomposites exhibited XRD plots, which resembled those of polydicyclopentadiene containing no clay (Figure 1). Gilman pointed out that XRD analysis alone can lead to false interpretations of

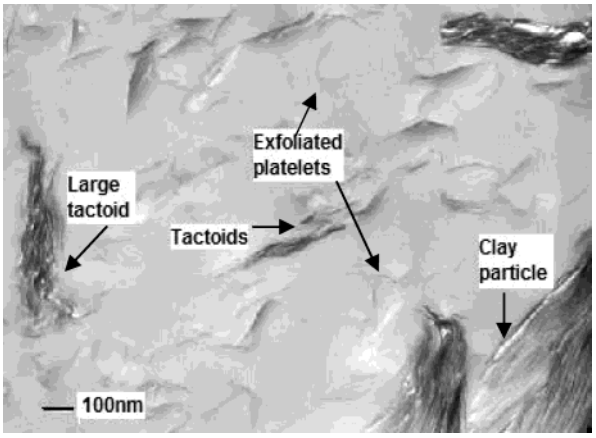

Figure 2. PolyDCPD contains 0.5 wt % clay I-28 after 1 h sonication.

hour sonication.

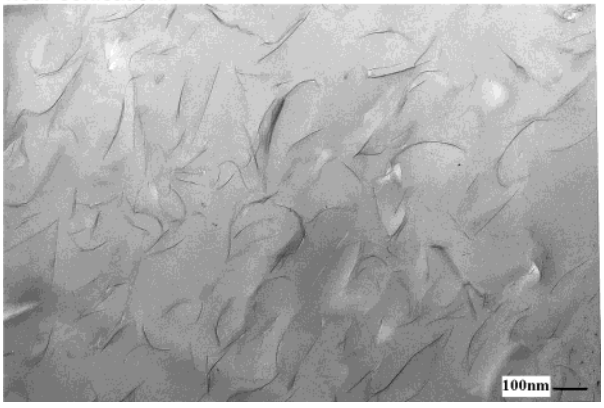

Figure 3. Highly delaminated 0.5 wt % I-28/PolyDCPD nanocomposite. The clay I-28/DCPD suspension was sonicated for 3 h, followed by curing (magnification 50 000).

the extent of exfoliation.[21,22] Thus, TEM studies are necessary to verify the extent of delamination and exfoliation achieved.[21,22]

X-ray scattering methods give averaged correlation information in a far larger volume of sample than TEM. This disadvantage of TEM was partially overcome by studying several slices from a sample and examining a large area in each slice. TEM micrographs were obtained on 0.5 wt % I-28/polyDCPD nanocomposites vs a series of sonication times employed before curing. After sonicating 1 h (Figure 2), clay nanolayers and tactoids have started to separate from the original clay particles. Some large tactoids are observed together with a small fraction of exfoliated individual platelets and some very small tactoids. Clay particles, however, are still clearly evident. The TEM of a 0.5 wt % I-28 sample which had been sonicated for 3 h is shown in Figure 3. This is a highly exfoliated nanocomposite, and no clay particles or large tactoids were evident after studying many TEM micrographs.

A small tactoid is observed in the upper center of Figure 3 where intercalation of polyDCPD into clay nanolayers is clearly evident. Most of the clay has been exfoliated into individual platelets or small tactoids of a few to 15 platelets thick. In this nanocomposite, clay nanolayers are relatively well dispersed. In this case, both XRD and TEM confirm that a highly delaminated clay/polyDCPD nanocomposite has been achieved.

Further characterization of the extent exfoliation of single 1 nm thick clay platelets was undertaken by

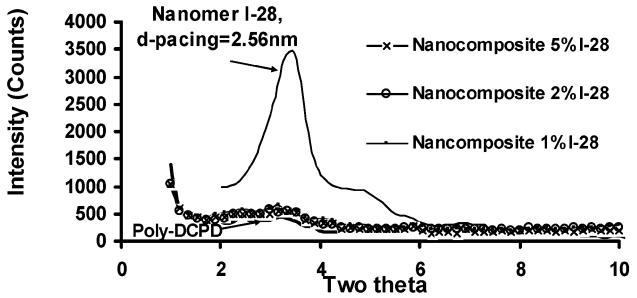

Figure 4. XRD plots of cured I-28 clay/polyDCPD composites containing from 0.5 to 5 wt % clay loadings but delaminated at a constant sonication time (3 h). Pure I-28 is shown for comparison.

detailed high-resolution TEM and neutron scattering techniques.[32] A preliminary analysis of small-angle neutron scattering (SANS) data was employed to fit the scattering data to a stacked disk model.[32−34] Nanocomposites with 0.5−2 wt % clay I-28 were studied. The slopes of scattering intensity, $I(Q)$, vs wave vector, Q, curves increased with increasing clay I-28 loading levels, indicating the average number of platelets per tactoid increased as the clay concentration went up when compared at equal sonication exposures. High-resolution TEM and SANS studies will be reported in detail elsewhere.[32]

The effect of increasing I-28 clay concentrations (from 0.5 to 5 wt %) on the extent of exfoliation at constant sonication (3 h) was also studied using TEM and by following changes in the d spacing by XRD. These samples were prepared by stirring clay into DCPD for 1 h and then sonicating for 3 h before curing. The XRD peak disappeared in each of the nanocomposites (0.5 wt % I-28 sample in Figure 1 and 1, 2, and 5 wt % I-28 samples in Figure 4). Increasing the clay concentration to 1, 2, 3, and 5 wt % at constant sonication time (3 h) generates more tactoids in the respective nanocomposites. A constant amount of sonication energy per unit time was delivered over the same length of time. As the wt % of I-28 was increased, this constant amount of input energy operated on more clay. Thus, the extent of nanodispersion and degree of exfoliation dropped as clay wt % increased. Furthermore, as nanodispersion progresses the viscosity increases, slowing the exfoliation process. Thus, at an equal degree of nanodispersion, the viscosity will be higher if the wt % of clay is higher.

Upon increasing the clay concentration to 2 wt % at 3 h of sonication (Figure 5a), significant exfoliation and a high degree of delamination were still observed. However, the maximum thickness of the small tactoids produced has increased to about 30 nm based on analyzing many TEM micrographs. Upon further increasing the concentration of clay I-28 to 3 and 5 wt %, highly delaminated nanocomposites continue to be obtained. These dispersions have a distribution containing single clay platelets and multilayer tactoids in the range 30−100 nm Figure 5b) and 50−150 nm (Figure 5c) thick for 3 and 5 wt % clay concentrations, respectively.

Average tactoid thickness increases with higher clay loadings at constant sonication. Detailed high-resolution TEM and neutron scattering studies of these tactoid distributions will be discussed elsewhere.[32]

Small-angle X-ray scattering (SAXS) was also employed to study clay I-28 and clay I-28/polyDCPD composites with clay loading levels of 0.5−2 wt %. The

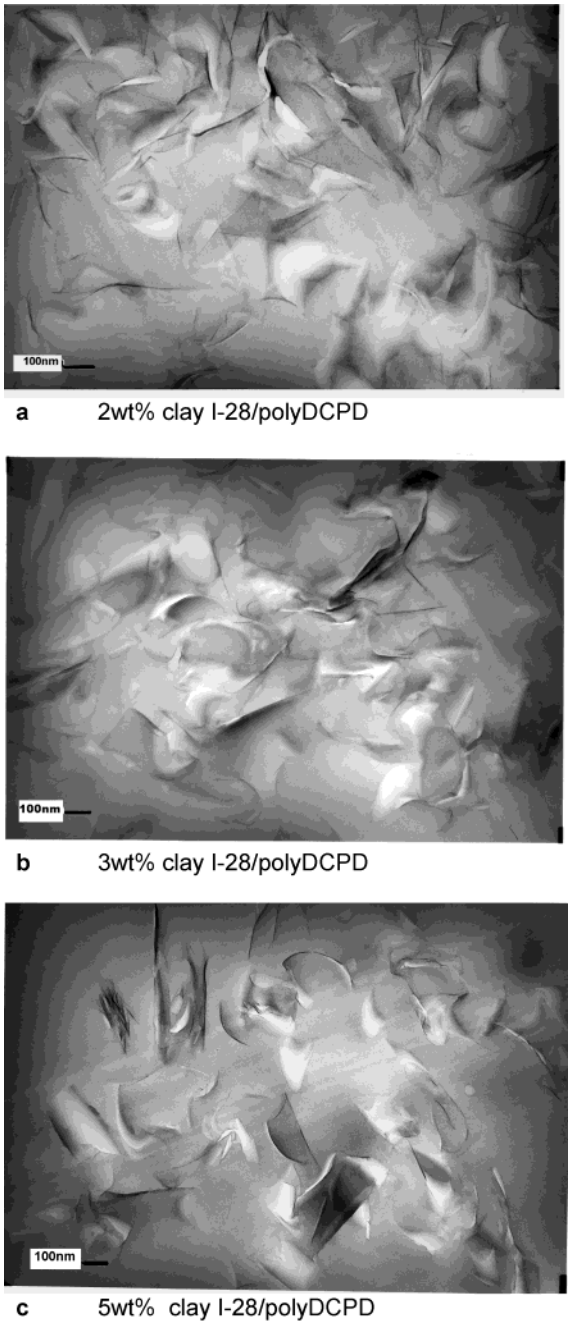

Figure 5. Representative TEMs of I-28/polyDCPD composites vs clay loading prepared using the same sonication time (3 h) in liquid DCPD prior to curing (at 50 000 magnification): (a**)** 2 wt % I-28 clay/DCPD, (b**)** 3 wt % clay I-28/polyDCPD, and **(**c**)** 5 wt % clay I-28/polyDCPD. All samples clay I-28/DCPD dispersions were sonicated for 3 h and then cured.

scattering from as-received clay I-28 powder exhibited a peak at $Q = 0.277$ Å^{-1}, corresponding to a clay platelet d spacing of $d = 2.24$ nm (Figure 6).

The I-28/polyDCPD composite scattering data were plotted as IQ^2 vs Q to better observe possible peaks related to ordered structures (Figure 7). Clay loadings from 0.5 to 2 wt % in polyDCPD were examined. No peaks indicating the existence of ordered structures in the Q region between 0.017 and 0.4 Å^{-1} were observed. This range corresponds to d spacings from 15.7 to 396 Å.

Clay I-44pa was dispersed into DCPD only by stirring for 1 h (without sonication). Then these dispersions were polymerized. No significant XRD peak was observed

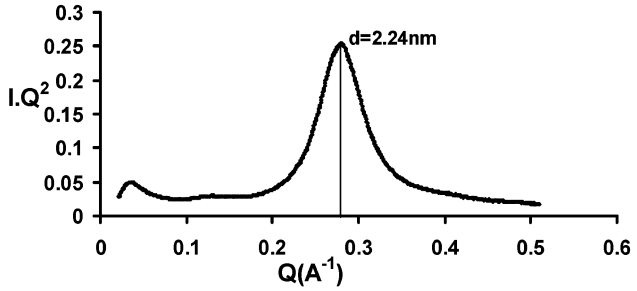

Figure 6. Small-angle X-ray scattering of I-28 clay powder.

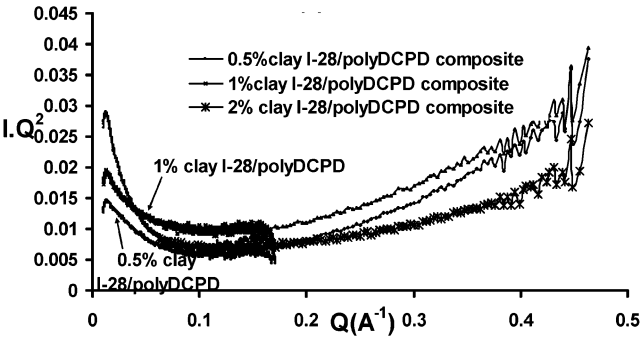

Figure 7. Small-angle X-ray scattering of clay I-28/polyDCPD composites.

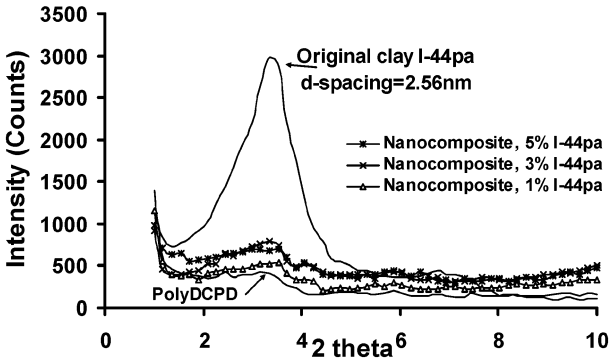

Figure 8. XRD of Nanomer I-44pa clay and its 0.5−5 wt % clay/polyDCPD nanocomposites prepared by stirring clay into DCPD and curing.

corresponding to ordered clay structures in the cured samples, even when the I-44pa loading was increased to 5 wt % (Figure 8). Therefore, the extent of nanodispersion achieved upon simple stirring of I-44pa appears substantially greater than that of I-28 according to XRD observations. In contrast, the I-28 swelled to a d spacing of 4.15 nm but exhibited an intense well-formed peak after stirring into DCPD (Figure 1). The high intensity of this peak indicates a large amount of the clay exists in particles and larger tactoids with reasonably well ordered stacking of platelets. I-44pa was pillared with dimethyldidecylammonium ions (155 mequiv/100 g of clay vs uptake of 132 mequiv/100 g of clay trimethyloctadecylammonium ions in clay I-28). These values were calculated from a carbon analysis assuming all carbon in the sample came from the ion exchange, so they represent maximum values. The ion exchange capacities are not supplied by Nanocor Inc. but are considered proprietary. They are in the range 120−160 mequiv/100 g of clay based on the sodium bentonite clay from which they are prepared. The disappearance of the I-44pa XRD peak suggests some greater degree of nanodispersion. Nevertheless, TEM and other techniques are required to definitely determine if more

highly delaminated I-44pa structures were actually formed.[21,22]

Representative TEM micrographs of a polyDCPD/0.5 wt % I-44pa sample are shown in Figure 9a,b. These TEMs clearly demonstrate that highly delaminated or exfoliated nanocomposites were not achieved, even at the lowest (0.5 wt %) clay loadings. Although the XRD scan does not show a clear peak corresponding to basal diffraction, the TEM micrographs show that clay exists in partially ruptured and partially intercalated particles with overall dimensions up to a few microns together with some large tactoids. However, very little exfoliation was found. The XRD instrument used could detect the d spacing at 2θ angles as small as 1.5°. This corresponds to 5.87 nm ordered layer structures. Expansions between the clay layers beyond the small-angle detecting range of XRD could result of the XRD peak loss. Alternatively, the sample's form, either as a powder or solid smooth surface, may change the orientation of ordered structure. Disordered or poorly ordered clay stacking can cause the disappearance of basal reflection peak.[21,22] Also, mixtures of various layer spacings within tactoids reduces and broadens any XRD peaks. In general, nanodispersed clay tactoids appear too disordered to give coherent scattering, even when platelet layers remain stacked within tactoids. Thus, careful examination of the I-44pa clay/polyDCPD composites demonstrated that the extent of exfoliation/delamination of clay nanolayers must be determined by the use of TEM and other methods which supplement the use of XRD.[21,22]

Viscoelastic Properties. The viscoelastic properties of polyDCPD and its highly delaminated clay nanocomposites were determined on samples that had been cured as described in the Experimental Section and then postcured at 280 °C for 2 h. These samples have a high cross-link density. The glass transition temperature (T_g defined at the tan δ peak) of the neat polyDCPD was 259 °C at 10 Hz and 257 °C at 1 Hz (Figure 10). The T_g of the 0.5 wt % I-28 clay nanocomposite was higher: 274 °C at10 Hz and 270 °C at 1 Hz. This significant increase (13−15 °C) for such a small amount of clay reflects the highly delaminated nature of this sample. The tan δ plots at 10 Hz for the composites with 0.5, 2, and 3 wt % I-28 are shown in Figure 10. The T_g values for both 2 and 3 wt % clay samples were close (258 and 254 °C at 10 Hz and 254 and 252 °C at 1 Hz, respectively) to those for the neat polyDCPD.

As the clay loading increased, the intensity of the bending tan δ peaks increased (Figure 10), indicating an increase in chain motion freedom. The degree of clay delamination within the polyDCPD matrix decreases as clay loading goes up. More large tactoids are present. Individual exfoliated clay platelets or very small tactoids have higher aspect ratio and higher surface areas per unit weight than large tactoids and particles. They appear more effective than large tactoids at restricting segmental motion. This may contribute to the higher T_g for the more highly delaminated 0.5 wt % clay sample. However, the degree of cure is dependent on both ruthenium-catalyzed ring-opening metathesis and complex thermal reactions. The ruthenium carbene catalyst is destroyed between 180 and 215 °C. The effect of clay platelet surfaces on the operation of the catalyzed ROMP and thermal cross-linking is unknown.

The bending storage moduli, E', of all the I-28 clay/polyDCPD nanocomposites were greater than those of

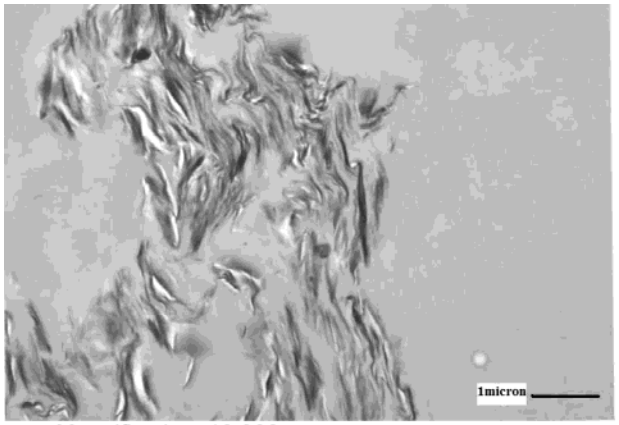

a Magnification: 10,000

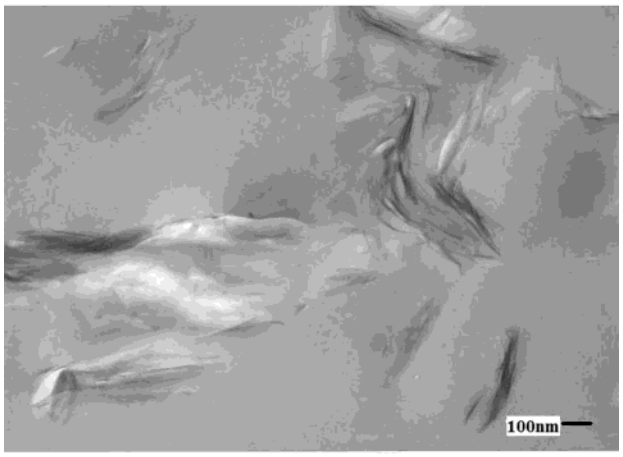

b Magnification: 40,000

Figure 9. TEM of a 0.5 wt % I-44pa/PolyDCPD composite. The clay was mechanically stirred in DCPD for 1 h prior to curing. Clay particles still exist with some tactoids.

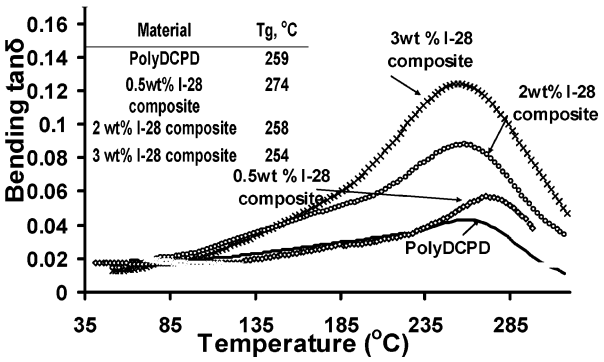

Figure 10. Bending tan δ vs temperature response of polyDCPD and I-28/polyDCPD nanocomposites (at 10 Hz).

polyDCPD from 40 °C to above 220 °C, at both 1 and 10 Hz (Figure 11). The E' values at 50 °C for pure polyDCPD and the 0.5 and 3 wt % I-28 composites were 0.813, 1.622, and 1.863 GPa, respectively. At temperatures up to ∼180 °C, samples with higher clay loadings (to 3 wt %) had somewhat higher bending moduli at both 1 and 10 Hz (Figure 11). This modulus remained higher than that of polyDCPD for the 0.5 wt % I-28 composite to above 285 °C while the modulus of the 5 wt % I-28 composite dropped below that of polyDCPD around 240 °C.

The flexural moduli, E_f, and flexural strengths, F_s, of polyDCPD and its I-28 clay nanocomposites were examined using the three-point bending test. Equation 1

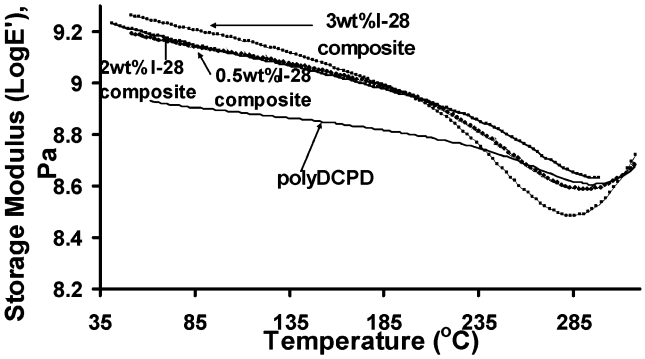

Figure 11. Viscoelastic bending response; the storage modulus of the polyDCPD and clay I-28/polyDCPD at 10 Hz.

Table 1. Flexural Moduli and Flexural Strengths of PolyDCPD and I-28/PolyDCPD Nanocomposites

material	flexural modulus (MPa)	flexural strength (MPa)
polyDCPD	3731	22.5
0.5 wt % I-28 composite	3937	52.9
1 wt % I-28 composite	4362	62.13
2 wt % I-28 composite	3992	53.17
3 wt % I-28 composite	3879	21.64

was employed, and linear viscoelastic behavior was assumed for the flexural moduli.[35] Flexural strength was calculated using eq 2.

$$E_f = \frac{L^3 P}{4bd\Delta} \quad (1)$$

$$F_s = \frac{3PL}{2bd\Delta} \quad (2)$$

In eqs 1 and 2, L is the length, b the width, d the thickness, P the maximum force, and Δ the maximum deflection.

The flexural moduli of all I-28 nanocomposites were higher than the 3731 MPa value of the pure polyDCPD (Table 1). The flexural moduli of the nanocomposites increased from 3937.1 MPa (0.5 wt % I-28) to 4361.8 MPa (1 wt % I-28). However, further increases in clay loading to 2 and 3% decreased moduli to 3992 and 3879 MPa, respectively. The 1 wt % clay nanocomposite had both highest flexural modulus and flexural strength. The flexural strength increased from 22.5 to 52.9 MPa by the addition of only 0.5 wt % I-28. This further increased to 62.1 MPa in the 1 wt % I-28 sample. As clay loading continued to increase, the flexural strengths dropped to 53.2 MPa for 2 wt % clay and then drastically to 21.6 MPa for 3 wt % clay.

The drops observed in flexural moduli and strengths correspond to a drop in the extent of clay delamination found with higher clay loading (especially in the 3 wt % clay sample). If all of the composites were as highly delaminated as the 0.5 wt % sample and the spatial dispersion was excellent, the flexural moduli and strengths might continue to increase as the wt % of clay went up. However, as the clay loading goes up, the extent of exfoliation/delamination dropped. The loading trends vs the extent of exfoliation/delamination operate in opposite directions, causing the mechanical properties to peak at about 1 wt % I-28. Superb enhancements in the strength and moduli might result if 3−5 wt % I-28 samples could be exfoliated and nanodelaminated to the same extent as the 0.5 wt % sample. Since the presence of clay influences the cure process (Figure 10), a single variable cannot be isolated to account for the observed property changes.

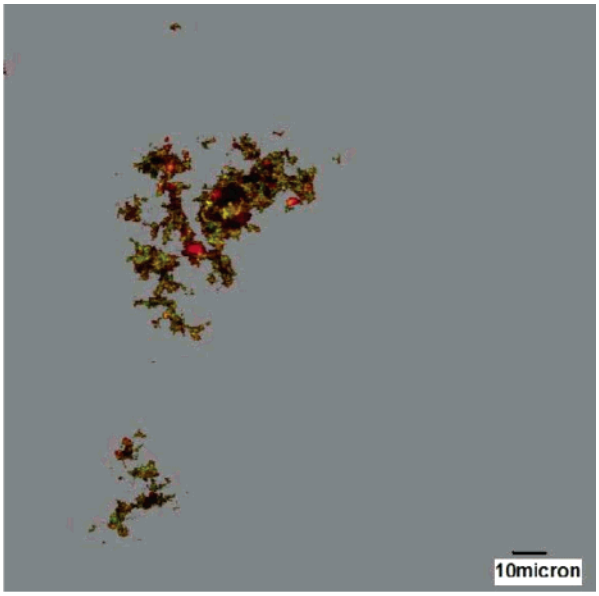

Figure 12. Confocal laser microscopy of the 1 wt % Safranine O-exchanged clay I-28 particles in DCPD after clay was stirred in the monomer 1 h.

Fluorescence Study of Clay Dispersion. Safranine O-tagged I-28 clay particles in DCPD liquid dispersions were studied by confocal laser microscopy. Figure 12 shows Safranine O-exchanged clay I-28 particles after stirring for 1 h in DCPD monomer. Safranine O has an ammonium ion function, which enables some of this dye to intercalate into the clay via cation exchange reaction. The 1 wt % I-28 clay/DCPD suspensions were studied after DCPD had been imbibed into the tagged clay's galleries during mechanical mixing. The same dispersions were also studied after sonicating the tagged clay/DCPD dispersion for 3 h to give the largest degree of clay delamination.

Safranine O is widely used as a fluoroprobe in confocal laser microscopy studies, acting as a counterstain.[31,36,37] At laser wavelengths of 476, 488, and 568 nm, the Safranine O-tagged clay which had been mechanically stirred in DCPD for 1 h is observed by its emitted green light. Excess Safranine O particles are observed as red spots (Figure 12). The clay in this sample still largely exists in particulate form with some large tactoids. However, after dispersion was promoted by 3 h of sonication, green emissions were seen as spots with diameters decreasing into the nanometer size range using the highest instrumental magnification (2000×) (Figure 13). Excess Safranine O, precipitated as particles in DCPD, were observed as larger red spots. Fluorescence labeling is one convenient method to follow the delamination process in the monomer as a function mixing conditions prior to curing. TEM can only be used after curing the monomer. At a numerical aperture of 1.4, the smallest image field possible on this instrument was 12 by 12 μm. Using a sampling frequency of 49 nm and a resolution/sampling frequency ratio of 2.8, a resolution limit of about 130 nm is achieved. The intensity of the green emission was sufficient to detect much smaller clay tactoids (estimate of 20 nm), but when detected, they could not be displayed as having the smaller size due to the ∼130 nm resolution limit.

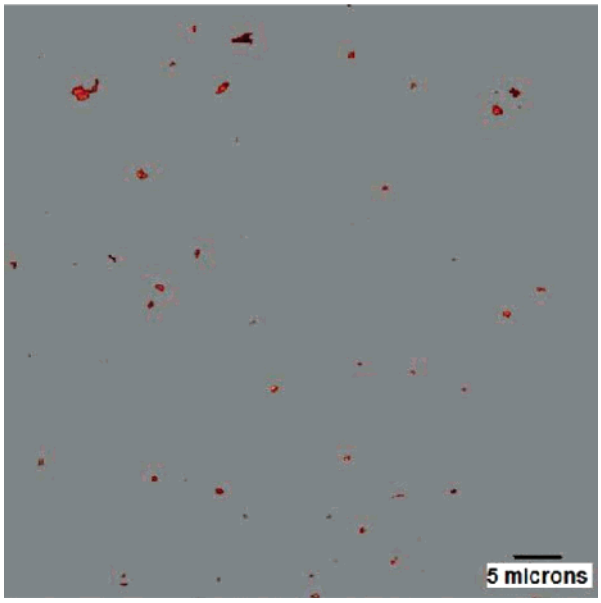

Figure 13. Highly delaminated 1 wt % Safranine O-exchanged I-28 clay particles in the clay I-28/DCPD dispersion after 3 h of sonication.

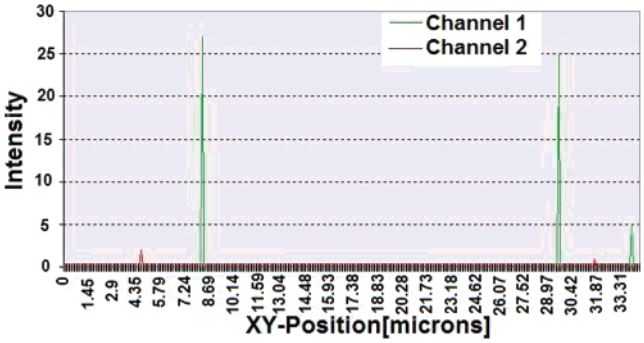

Figure 14. Intensity of green and red emission vs the particle lengths of a 1 wt % I-28 clay/DCPD monomer dispersion after 3 h of sonication.

The largest clay particle size detected after sonicating for 3 h was 135 nm.

Conclusions

Highly delaminated clay nanodispersions and nanocomposites can be synthesized in the highly nonpolar hydrophobic monomer DCPD and polyDCPD. The degree of delamination was examined by XRD, SAXS, and TEM. Confocal laser microscopy with a fluorescent probe for the first time was used to study the clay I-28/liquid DCPD dispersion. XRD cannot be used alone as a criterion to determine whether highly delaminated composites have been obtained or that exfoliation has been achieved. In mechanically mixed I-44pa clay/polyDCPD samples, no XRD peaks relevant to an ordered structure were present, but TEM studies demonstrated that clay particles still exist and highly delaminated nanocomposites were not achieved.

It is clear that highly delaminated nanocomposites, where tactoids exist having 2−15 platelets, represent a different class of composites than fully exfoliated or intercalated systems. We emphasize this distinction between a fully exfoliated system, in which all platelets are noninteracting (at large distances from each other) and highly delaminated nanocomposites where small tactoid stacks containing 2 to ∼15 individual platelets are well dispersed along with some exfoliated platelets.

The 2 to ∼15 clay platelet layers of small tactoids could be observed by TEM in the highly nanodispersed, low wt % clay samples. However, the XRD and SAXS peak, clearly observed in the original clay particles, disappeared as nanodispersion advanced. This occurs because the nanodispersed systems are too disordered to give coherent scattering.[21,22] It is well-known that minerals may produce somewhat irrational reflections if the crystallites are exceedingly thin (less than 10 unit cells per crystallite).[38] This situation is common with clay minerals and must be true as large tactoids get smaller. Size effects have been noted by Mering,[39] MacEwan et al.,[40] Reynolds,[41] Ross,[42] and Trunz.[43] Thin tactoids are frequently curved. This buckling can contribute to irregularities in the interlayer spacing. In addition, layer spacings may vary slightly based on whether those layers underwent ion exchange with the quaternary ammonium pillars. Also, the ends of these small tactoids frequently are partially splayed apart as some platelet separation is beginning to occur due to monomer infusion. Such partial disordering and the relative abundances of these components will cause reflection spacings to be more irrational. The low (<3%) weight percent of clay present is another major contributor. This magnifies the loss of a distinct peak, caused by all the other factors reducing coherent scattering.

The glass transition temperature of the highly delaminated polyDCPD/0.5 wt % I-28 clay sample increased about 13 °C compared to the T_g of pure polyDCPD. The extent of delamination/exfoliation dropped as the wt % of clay increased at constant sonication energy input. The presence of larger tactoids and particles did not significantly contribute to raising T_g, E', E_f, or the flexural strength. Thus, the enhancement of properties was maximized at ∼1 wt % clay (∼0.5 wt % clay for T_g). Some properties of the composites actually decreased relative to pure polyDCPD at high clay loadings where the degree of nanodelamination was poor. For example, the largest increase in flexural modulus and flexural strength was observed at 1 wt % clay loading level, but at 3 wt % clay the flexural strength was slightly less than polyDCPD.

Clay dispersions were tagged with the fluorescent dye, Safranine O, by ion exchange into clay galleries at the particulate stage. Confocal microscopy was then used after 3 h of sonication to follow delamination/dispersion of clay within the liquid monomer during mixing or sonication, prior to curing. Thus, the extent of nanodispersion could be followed down to a size of ∼130 nm prior to curing. While the resolution is not as good as TEM, this method can be employed to follow the mixing process for quality control.

Acknowledgment. The authors acknowledge the award of a Honda Fellowship to M. Yoonessi by the Bagely College of Engineering. The Air Force Office of Scientific Research (Grant F49620-02-1-026-0) and the National Science Foundation (Grant EPS0132618) provided financial support for this work. Dr. J. S. Lin of Oak Ridge National Laboratory is thanked for running SAXS experiments and expert interpretation.

References and Notes

(1) (a) Ren, J.; Krishnamoorti, R. *Macromolecules* **2003**, *36*, 4443−4451. Ballard, R. L.; Tuman, S. J.; Fouquette, D. J.;

Stegmiller, W.; Soucek, M.; D. *Chem. Mater.* **1999**, *11*, 726−735. (b) Patton, R. D.; Pittman, C. U., Jr.; Wang, L.; Hill, J. R.; Day, A. *Composites, Part A* **2001**, *5*, 1−9. (c) Matsumura, T.; Ochi, M.; Nakata, K. *J. Appl. Polym. Sci.* **2003**, *90*, 1980−1984. (d) Shang, X.; Zhu, Z.; Yin, J.; Ma, X. *Chem. Mater.* **2002**, *14*, 71−77. (e) Nawala, H. S. *Handbook of Organic−Inorganic Hybrid Materials and Nanocomposites*; American Scientific Publishers: Stevenson Ranch, CA, 2003. (f) Gomez-Romero, P.; Sanchez, C. *Functional Hybrid Materials*; Wiley-VCH: Wienheim, Germany, 2003. (g) Mark, J. E.; Lee, C. C.-Y.; Bianconi, P. A. *Hybrid Organic−Inorganic Composites*; American Chemical Society: Washington, DC, May 1995.

(2) (a) Yoshihara, M.; Oie, H.; Okada, A.; Matsui, H.; Ohshiro, S. *Macromolecules* **2002**, *35*, 2435−2436. (b) Nawala, A. S. *Encyclopedia of Nanoscience and Nanotechnology*; American Scientific Publishers: Stevenson Ranch, CA, March 2003. (c) Laine, R. M., Ed.; *Materials Research Society Symposia Proceedings*, Vol. 628, Organic/Inorganic Hybrid Material, 2000: Symposium April 24−28, San Francisco, CA. (c) Harreld, J. H.; Esaki, A.; Stucky, G. D. *Chem. Mater.* **2003**, *15*, 3481−89. (d) Chen, Y.; Iroh, J. O. *Chem. Mater.* **1999**, *11*, 1218−1222.

(3) Tamaki, R.; Choi, J.; Laine, R. M. *Chem. Mater.* **2003**, *15*, 793−797.

(4) Pyun, J.; Matyjaszewski, K.; Kowalewski, T.; Savin, D.; Patterson, G.; Kickelbick, G.; Huesing, N. *J. Am. Chem. Soc.* **2001**, *123*, 9445−9446.

(5) Li, G. Z.; Wang, L.; Toghiani, H.; Daulton, T. L.; Koyama, K.; Pittman, C. U., Jr. *Macromolecules* **2001**, *34*, 8686−8693.

(6) He, J.-A.; Valluzzi, R.; Yang, K.; Dolukhanyan, T.; Sung, C.; Kumar, J.; Tripathy, S. K.; Samuelson, L.; Balogh, L.; Tomalia, D. A. *Chem. Mater.* **1999**, *11*, 3268−3274.

(7) Percy, M. J.; Barthet, C.; Lobb, J. C.; Khan, M. A.; Lascelles, S. F.; Vamvakaki, M.; Armes, S. *Langmuir* **2000**, *16*, 6913−6920.

(8) Patton, R. D.; Pittman, C. U., Jr.; Wang, L.; Hill, J. R. *Composites, Part A* **1999**, *30*, 1081−1091.

(9) Lan, T.; Pinnavaia, T. J. *Chem. Mater.* **1994**, *6*, 2216−2219.

(10) Messersmith, P. B.; Giannelis, E. P. *J. Polym. Sci., Part A: Polym. Chem.* **1995**, *33*, 1047−57.

(11) Brown, J. M.; Curliss, D.; Vaia, R. A. *Chem. Mater.* **2000**, *12*, 3376−3384.

(12) (a) Gilman, J. W.; Jackson, C. L.; Morgan, A. B.; Harris, R., Jr.; Manias, E.; Giannelis, E. P.; Wuthenow, M.; Hilton, D.; Philips, S. H. *Chem. Mater.* **2000**, *12*, 1866−1873. (b) Zhu, J.; Morgan, A. B.; Lamelas, F. J.; Wilkie, C. A. *Chem. Mater.* **2001**, *13*, 3774−3780. (c) Triantafillidis, C. S.; LeBaron, P. C.; Pinnavaia, T. J. *Chem. Mater.* **2002**, *14*, 4088−4095.

(13) Zhu, J.; Wilkie, C. A. *Polym. Int.* **2000**, *49*, 1158−1163. Zhao, Z.; Tang, T.; Qin, Y.; Huang, B. *Langmuir* **2003**, *19*, 7157−59.

(14) Messersmith, P. B.; Giannelis, E. P. *J. Polym. Sci., Part A: Polym. Chem.* **1995**, *33*, 1047−1057. Pinnavaia, T. J.; Beall, G. *Polymer-Clay Nanocomposites*; John Wiley & Sons: Hoboken, NJ, March 2001.

(15) Chin, I.; Thurn-Albretcht, T.; Kim, H.; Russel, Th. P.; Wang, J. *Polymer* **2001**, *42*, 5947−5952.

(16) (a) Krishnamarooti, R.; Vaia, R. A.; Giannelis, E. P. *Chem. Mater.* **1996**, *8*, 1728−1734. (b) Ishida, H.; Campbell, S.; Blackwell, J. *Chem. Mater.* **2000**, *12*, 1260−1267.

(17) Morgan, A. B.; Gilman, J. W.; Jackson, C. L. *Macromolecules* **2001**, *34*, 2735−2738.

(18) (a) Brindley, G. W. In *Crystal Structures and Their X-Ray Identification*; Mineralogical Society No. 5; Brindley, G. W., Brown, G., Eds.; London, 1984; pp 169−172. (b) Brown, G.; Brindley, G. W. In *Crystal Structures and Their X-RayIdentification*; Mineralogical Society No. 5; Brindley, G. W., Brown, G., Eds.; London, 1984; pp 305−350.

(19) Cao, G.; Mallouk, T. E. *J. Solid State Chem.* **1991**, *94*, 59.

(20) Mehrotra, V.; Giannelis, E. P. *Solid State Commun.* **1991**, *77*, 155.

(21) Morgan, A. B.; Gilman, J. W.; Jackson, C. L. *Proceedings of the American Chemical Society: Polymeric Materials Science & Engineering*, Vol. 82, San Francisco, CA, March 2000; American Chemical Society: Washington, DC, 2000; pp 270−271.

(22) Gilman, J. W.; Morgan, A. B. *J. Appl. Polym. Sci.* **2003**, *87*, 1329−1338.

(23) Hanlin, N. Master Thesis, Mississippi State University, 2002.

(24) Mariani, A.; Fiori, S.; Chekanov, Y.; Pojman, J. A. *Macromolecules* **2001**, *34*, 6539−6541.

(25) Zhang, D.; Huang, J.; Qian, Y.; Chan, A. S. C. *J. Mol. Catal. A: Chem.* July **1998**, *133*, 135−138.

(26) Trnka, T. M.; Grubbs, R. H. *Acc. Chem. Res.* **2001**, *34*, 18−29.

(27) Bielawski, C. W.; Benitez, D.; Grubbs, R. H. *J. Am. Chem. Soc.* **2003**, *125*, 8424−8425.

(28) Wignall, G. D.; Lin, J. S.; Spooner, S. *J. Appl. Crystallogr.* **1990**, *23*, 241−245.

(29) Schelten, J. R.; Hendricks, W. *J. Appl. Crystallogr.* **1978**, *11*, 297−324.

(30) Russell, T. P.; Lin, J. S.; Spooner, S.; Wignall, G. D. *J. Appl. Crystallogr.* **1988**, *21*, 629.

(31) Santos, P. D.; Kowaltowski, A. J.; Laclau, M. N.; Seetheraman, S. S.; Paucek, Boudina, S.; Thambo, J. B.; Tariosse, L.; Garlid, K. D. *Am. J. Physiol. Heart Circ. Physiol.* **2002**, *238*, H284−H295.

(32) Yoonessi, M.; Toghiani, H.; Kim, M. H.; Lin, J. S.; Daulton, T. L.; Pittman, C. U., Jr. Manuscript in preparation.

(33) Glinka, C. J. *Summer School Notes on Neutron Scattering and Reflectometry from Submicron Structures*, NIST Center for Neutron Research, June 3−7, 2002.

(34) Ho, D. L.; Briber, R. M.; Glinka, C. J. *Chem. Mater.* **2001**, *13*, 1923−1931.

(35) McCrum, N. G.; Buckley, C. P.; Bucknall, C. B. *Principles of Polymer Engineering;* Oxford University Press: New York, 1988; p 344.

(36) Lu, Y.; Edwards, R. B., III; Kalascheur, V. L.; Nho, S.; Cole, B. J.; Markel, M. D. *47th Annual Meeting, Orthopeadic Resaerch Society*, Feb 25−28, 2001, San Francisco, CA.

(37) Karanastasi, E.; Vellios, E.; Roberts, I. M.; MacFarlane, S. A.; Brown, D. J. F. *Nemathology* **2000**, *2*, 237−245.

(38) Reynolds, R. C. In the *Crystal Structures and Their X-Ray Identification*; Mineralogical Society No. 5; Brindley, G. W., Brown, G., Eds.; London, 1984; Chapter 4, pp 249−302.

(39) (a) Mering, J. *Acta Crystallogr.* **1949**, *2*, 371−377. (b) Mering, J. *Proc. 4th Int. Congr. Soil Sci., Amsterdam* **1950**, *3*, 21−26.

(40) (a) MacEwan, D. M. C. *Kolloidzeitschrift* **1956**, *149*, 96−108. (b) MacEwan, D. M. C.; Ruitz, A. A. Interstratified Clay Minerals. In *Soil Components*, Vol. 2, *Inorganic Components;* Gieseking, J. E., Ed.; Springer-Verlag: New York, 1975. (c) MacEwan, D. M. C.; Ruitz, A. A.; Brown, G. Interstratified Clay Minerals. In the *X-Ray Identification and Clay Structures of Clay Minerals*; Brown, G., Ed.; Mineralogical Society: London, 1961.

(41) (a) Reynolds, R. C. *Acta Crystallogr.* **1968**, *A24*, 319−320. (b) Reynolds, R. C. *Geochim. Acta* **1963**, *27*, 1097−1112. (c) Reynolds, R. C. *Am. Mineral.* **1965**, *50*, 990−1001. (d) Reynolds, R. C. *Am. Mineral.* **1967**, *52*, 661−672. (d) Reynolds, R. C. *Clays Clay Mineral.* **1971**, *19*, 361−374. (e) Reynolds, R. C. *Am. Mineral.* **1976**, *61*, 484−491. (f) Reynolds, R. C. *Clays Clay Mineral.* **1970**, *18*, 25−36.

(42) Ross, M. *Z. Kristallogr. Kristallgeom.* **1968**, *126*, 80−97.

(43) Trunz, V. *Clays Clay Mineral.* **1976**, *24*, 84−87.

MA0359483